RSC Advances

RSC Publishing

PAPER

View Article Online
View Journal | View Issue

Cite this: *RSC Adv.*, 2013, **3**, 20816

Polyvinyl alcohol (PVA)–cellulose nanofibril (CNF)–multiwalled carbon nanotube (MWCNT) hybrid organic aerogels with superior mechanical properties

Qifeng Zheng,[ab] Alireza Javadi,[bc] Ronald Sabo,[d] Zhiyong Cai*[d] and Shaoqin Gong*[abc]

Received 10th May 2013
Accepted 27th August 2013

DOI: 10.1039/c3ra42321b

www.rsc.org/advances

Polyvinyl alcohol (PVA)–cellulose nanofibril (CNF)–multiwalled carbon nanotube (MWCNT) hybrid organic aerogels were prepared using an environmentally friendly freeze-drying process with renewable materials. The material properties of these "green" hybrid aerogels were characterized extensively using various techniques. It was found that adding a small amount of CNFs and MWCNTs increased the mechanical properties of the PVA aerogels drastically. The mechanical properties of the hybrid aerogels showed an exponential dependency on the relative aerogel densities. These low-density hybrid aerogels also exhibited very low thermal conductivities and high surface areas, thereby making them potentially useful for many applications including thermal insulation and structural components.

Introduction

Aerogels are light-weight solid materials prepared by a process that replaces the liquid solvent in the gel with air without substantially altering the network structure or the volume of the gel body.[1] Aerogels possess many remarkable properties, including ultralow density (4–500 kg m^{-3}), high porosity, high specific surface area, and low dielectric constant, as well as extraordinarily low thermal conductivity.[2] The combination of these unusual properties makes aerogels attractive for a wide range of applications[2–12] including thermal and acoustic insulation,[4,5] catalyst supports,[7] drug release,[8,9] structural components,[10] and energy storage.[11,12]

Cellulose is the most abundant and renewable natural polymer and is biocompatible and biodegradable.[13] Cellulose nanofibrils (CNFs) have high surface areas and high aspect ratios, thus they can easily form an entangled web-like structure. CNFs also exhibit excellent flexibility and outstanding mechanical properties.[14,15] CNFs can be fabricated using various methods including mechanical shearing,[16,17] 2,2,6,6-tetramethylpiperidine-1-oxyl (TEMPO)-mediated oxidation,[18,19] enzymatic hydrolysis of macroscopic fibers followed by high-pressure homogenization,[20,21] or ultrasonication.[22,23] CNF aerogels have been reported by a number of groups. They generally exhibit ultralow density, high flexibility, high surface areas, and low thermal conductivities.[16,24–27] In spite of these intriguing properties, CNF aerogels generally possess inferior strength and modulus.[28] Therefore, several strategies have been adopted to improve the mechanical strength and modulus of the CNF-based aerogels including incorporation of inorganic fillers, such as silica,[29,30] and chemically crosslinking the CNFs utilizing the abundant hydroxyl groups present on the surfaces of CNFs.[2]

Carbon nanotubes (CNTs) are among the strongest materials known today.[31] Previous studies have demonstrated that the addition of a small amount of CNTs to a polymer matrix can enhance its mechanical properties significantly when properly dispersed.[32,33] While non-functionalized CNTs typically are not soluble in aqueous solution, they can be dispersed very well in a CNF aqueous solution when the pH value is controlled between 6 and 10.[34] Moreover, both CNFs and MWCNTs have high aspect ratios, which can easily entangle and form a highly interconnected 3D network, thereby reinforcing the resulting the aerogels. Polyvinyl alcohol (PVA) has excellent water solubility and biocompatibility. It can also form strong interactions with CNFs *via* hydrogen bonding. CNFs were used as a nanofiller to reinforce solid PVA composites.[35,36] In this paper, we report a novel, ultralight, and mechanically robust polyvinyl alcohol (PVA)–cellulose nanofibril (CNF)–multiwalled carbon nanotube (MWCNT) hybrid organic aerogel fabricated using an environmentally friendly freeze-drying method.[37] The PVA, CNFs, and OH-functionalized MWCNTs were chemically crosslinked together *via* the hydroxyl groups present on these components using glutaraldehyde (*cf.* Fig. 1). The mechanical properties of these PVA–CNF–MWCNT hybrid aerogels were superior to those reported in the literature[38–42] for clay/cellulose aerogel,[39] epoxy/clay aerogels,[40] polymer/clay/nanotubes aerogels,[41] and polymer/

[a]*Material Science Program, University of Wisconsin-Madison, WI 53706, USA. E-mail: sgong@engr.wisc.edu; Tel: +1 6083164311*

[b]*Wisconsin Institute for Discovery, University of Wisconsin-Madison, WI 53715, USA*

[c]*Department of Biomedical Engineering, University of Wisconsin-Madison, WI 53706, USA*

[d]*Forest Product Laboratory, USDA, Madison, WI 53726, USA. E-mail: zcai@fs.fed.us; Tel: +1 6082319446*

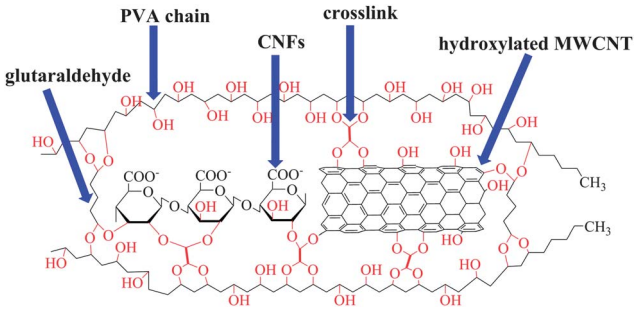

Fig. 1 A schematic illustration of the crosslinking mechanism.

silica aerogels[42] at comparable densities. Moreover, the mechanical properties demonstrated a strong exponential relationship with the relative aerogel densities, thereby making it possible to fabricate aerogels with a wide range of mechanical properties by adjusting the relative aerogel densities.

Experimental

Materials

The cellulose used for producing the CNFs was a commercially supplied fully bleached eucalyptus kraft pulp. PVA (MW ~ 95 000 g mol^{-1}), glutaraldehyde (GA, crosslinker, 25 wt% in H_2O), and 2,2,6,6-tetramethyl-1-piperidinyloxy (TEMPO, 98 wt %) were all obtained from Sigma Aldrich. Hydroxyl-functionalized MWCNTs (OH content: 3.70 wt%; aspect ratio: 1×10^3 to 4×10^3) were obtained from Cheap Tubes (Brattleboro, VT). Sodium chlorite, sodium bromide, sodium hypochlorite solution, and other chemicals were of laboratory grade (Fisher Scientific, USA) and used without further purification.

Preparation of CNFs

The TEMPO-oxidized CNFs used in this experiment were prepared according to a procedure described by Isogai's group.[19] Briefly, fully bleached eucalyptus fibers were oxidized with sodium hypochlorite using TEMPO as a catalyst at a temperature of 60 °C for 48 h. The fibers were then thoroughly washed and refined in a disk refiner with a gap of approximately 200 μm. The coarse fibers were separated by centrifuging at 12 000*g*, and the fine CNF dispersion was concentrated to 0.5 wt% using ultrafiltration. A final refining step was performed in which the nanofiber dispersion was passed through an M-110EH-30 microfluidizer (Microfluidics, Newton, MA) once with 200 and 87 μm chambers in series. The obtained CNF suspension was stored at 4 °C without any treatment before future utilization. The carboxylate content of the CNFs was measured *via* titration based on the TAPPI Test Method T237 cm-98 and was found to be 0.46 mmol COONa per gram of CNF suspension.

Preparation of high density PVA solution

Polyvinyl alcohol (10.0 g, MW: 95 000 g mol^{-1}) was dissolved in 100 mL of water and stirred for 12 h at 85 °C until the PVA was completely dissolved in water. Then, the PVA solution was used for the synthesis of aerogels.

Preparation of crosslinked PVA aerogels

PVA solution (5.0 mL, 0.1 g mL^{-1}) and a desired amount of water were mixed together in a flask under vigorous stirring for 1 h. Then, glutaraldehyde solution (250 μL, 25 wt%) and sulfuric acid (25 μL, 7.5 vol%) were added to the PVA solution. The resulting mixture was mixed under stirring for another hour. At the final stage, the mixture was sonicated in an ultrasonic bath for 10 min to obtain the aqueous gels. After being transferred into aluminum pans, the aqueous gel was crosslinked in a vacuum oven at 75 °C for 3 h. The PVA aerogels were fabricated using a freeze-drying process and were stored in a vacuum oven for further characterization.

Freeze-drying process

The crosslinked aqueous gels were precooled in a 4 °C refrigerator overnight to avoid macroscopic fracture during the freezing step, and were then frozen at −78 °C in a dry ice-acetone solution. The frozen samples were freeze-dried in a lyophilizer at a condenser temperature of −87.0 °C under vacuum (0.0014 mBar) for three days to produce the aerogels.

Preparation of crosslinked PVA–CNF aerogels

PVA solution (5.0 mL, 0.1 g mL^{-1}), CNF solution (20.0 g, 0.50 wt %), and a desired amount of water (depending on the specific density of the aerogels) were mixed together in a flask under vigorous stirring for 1 h. The weight ratio between the PVA and CNF was 5 : 1 for PVA–CNF samples. Then, glutaraldehyde solution (300 μL, 25 wt%) and sulfuric acid (30 μL, 7.5 vol%) were added to the PVA–CNF solution. The resulting mixture was mixed under constant stirring for another hour. At the final stage, the mixture was sonicated in an ultrasonic bath for 10 min to obtain the aqueous gels. After being transferred into aluminum pans, the aqueous gels were crosslinked/cured in a vacuum oven at 75 °C for 3 h. PVA–CNF aerogels were obtained using the freeze-drying process and were stored in a vacuum oven for further characterization.

Preparation of crosslinked PVA–CNF–MWCNT aerogels

The preparation process of the crosslinked PVA–CNF–MWCNT aerogels is shown schematically in Fig. 2. In a typical procedure, 25.0 mg of MWCNTs were added to a 50 mL centrifuge tube containing 10 mL of deionised water. The mixture was sonicated (UP400S, Hielscher USA) at 80% amplitude using a 3 mm probe in an ice-bath for 30 min. The resulting MWCNT aqueous solution was then mixed with 20.0 g of CNF aqueous dispersion (0.5 wt%) under sonication (10 min) to gives a homogeneous CNF–MWCNT mixture. Subsequently, 5.0 mL of PVA solution (0.1 g mL^{-1}) and a desired amount of water (depending on the specific formulation) were added into the flask containing the CNF–MWCNT aqueous solution under vigorous stirring for 1 h. The weight ratio between the PVA and CNF was 5 : 1 for all formulations. Thereafter, glutaraldehyde solution (300 μL, 25 wt %) and sulfuric acid (30 μL, 7.5 vol%) were added to the PVA–CNF–MWCNT solution, which was mixed under stirring for another hour. At the final stage, the mixture was subjected to

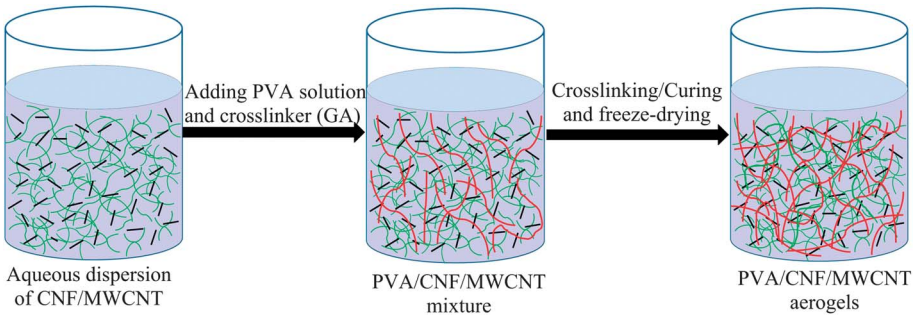

Fig. 2 Scheme of the preparation of crosslinked PVA–CNF–MWCNT aerogels.

sonication in an ultrasonic bath for 10 min to obtain the aqueous gels. After being transferred into aluminum pans, the aqueous gels were crosslinked/cured in a vacuum oven at 75 °C for 3 h. The aerogels were then prepared through a freeze-drying process and stored in a vacuum oven for further characterization. For all of the PVA–CNF–MWCNT aerogels, the ratio of each component was kept the same, namely, there was 4 wt% MWCNTs, 16 wt% CNFs, and 80 wt% PVA. Thus, the densities of the PVA–CNF–MWCNT aerogels were controlled by the amount of water added to the mixtures.

Characterization

All tests described below were done at least in triplicate and the average results as well as the standard deviations were reported. The densities of the aerogels were calculated by measuring the mass and volume of the aerogels. The densities of the solid materials (ρ_s) were calculated according to the solid density of each component and their weight ratios used in the formulation. The densities of the CNFs, MWCNTs, and PVA used for this study were 1460, 2100, and 1269 kg m^{-3}, respectively, according to the manufacturer's data sheet. Compression testing was conducted using an Instron (model 5967) fitted with a 30 kN load. The compression strain rate was set to 10% min^{-1}. Compression moduli were extracted from the slopes of the linear elastic deformation region of the stress–strain curves, while the yield stress was taken as the stress at the intersection between the tangent line to the linear elastic region and the tangent line of the plateau region. The microstructures of the aerogels were studied using a scanning electron microscope (SEM, NeoScope JCM-5000). The SEM samples were coated using gold sputtering. The Brunauer–Emmett–Teller (BET) specific surface area was determined by N_2 physisorption using a Gemini analyzer (Micromeritics, USA). It was measured by analyzing the amount of N_2 gas adsorbed on the samples with the relative vapor pressure (P/P_0) ranging from 0.05 to 0.3 at −196 °C. Thermal stability measurements were carried out using a thermogravimetric analyzer (TGA, Q 50 TA Instruments, USA) from room 30 °C to 600 °C at 10 °C min^{-1} heating rate under N_2 protection. The bulk thermal conductivity was measured using a thermal constants analyzer (ThermTest TPS 2500 S) following an ISO standard (ISO/DIS 22007-2.2), transient Plane Source method. Measurement time ranged from 40 to 80 seconds. The laboratory temperature was 20 ± 1 °C and the relative humidity was 22 ± 2% during the measurements. Five measurements were made on each formulation and the average values and the standard deviations were reported.

Results and discussion

Microstructures of the various aerogels

PVA, PVA–CNF, and PVA–CNF–MWCNT aerogels with four different densities were successfully prepared using the freeze-drying method. Under optimal processing conditions, very little shrinkage was observed in these aerogels compared to their initial hydrogel dimensions. Fig. 3 shows the microstructures of the various aerogels including (a) PVA (25.42 kg m^{-3}), (b) PVA–CNF (26.83 kg m^{-3}), and the PVA–CNF–MWCNT-1, 2, 3, and 4 hybrid aerogels with a density of (c) 14.55, (d) 20.13, (e) 26.00, and (f) 30.62 kg m^{-3}, respectively. All aerogels exhibited an interconnected, highly porous cellular structure. At similar densities (~26 kg m^{-3}), the pore sizes of PVA (Fig. 3(a), typically 3–8 μm) were somewhat larger than those of the PVA–CNF (Fig. 3(b), typically 2–5 μm) and PVA–CNF–MWCNT-3 (Fig. 3(e), typically 1–4 μm). This observation might be attributed to the fact that CNFs and/or MWCNTs could easily entangle and form a 3D network within the PVA–CNF or PVA–CNF–MWCNT aerogel network thereby affecting the nucleation and growth of ice crystals during the freeze-drying process. For the PVA–CNF–MWCNT aerogels with varying densities (Fig. 3(c)–(f)), the pore sizes appeared to be slightly smaller at higher aerogel densities. In addition, for the PVA–CNF and PVA–CNF–MWCNT hybrid aerogels, there were nanosized fibers connecting the sheet-like structures present in these hybrid aerogels. These highly interconnected 3D cellular networks may be responsible for the aerogels' outstanding mechanical properties.

BET surface areas of the aerogels

The BET specific surface area of the aerogels is shown in Table 1. The surface areas of the aerogels prepared by the freeze-drying process are often lower than those of aerogels prepared using supercritical CO_2 drying because the initial hydrogel network structure can be preserved better in aerogels prepared using supercritical drying compared to freeze-drying.[43]

At similar aerogel densities (~26 kg m^{-3}), incorporation of CNFs and MWCNTs (*i.e.*, PVA–CNF and PVA–CNF–MWCNT-3) significantly increased the specific surface areas of the PVA

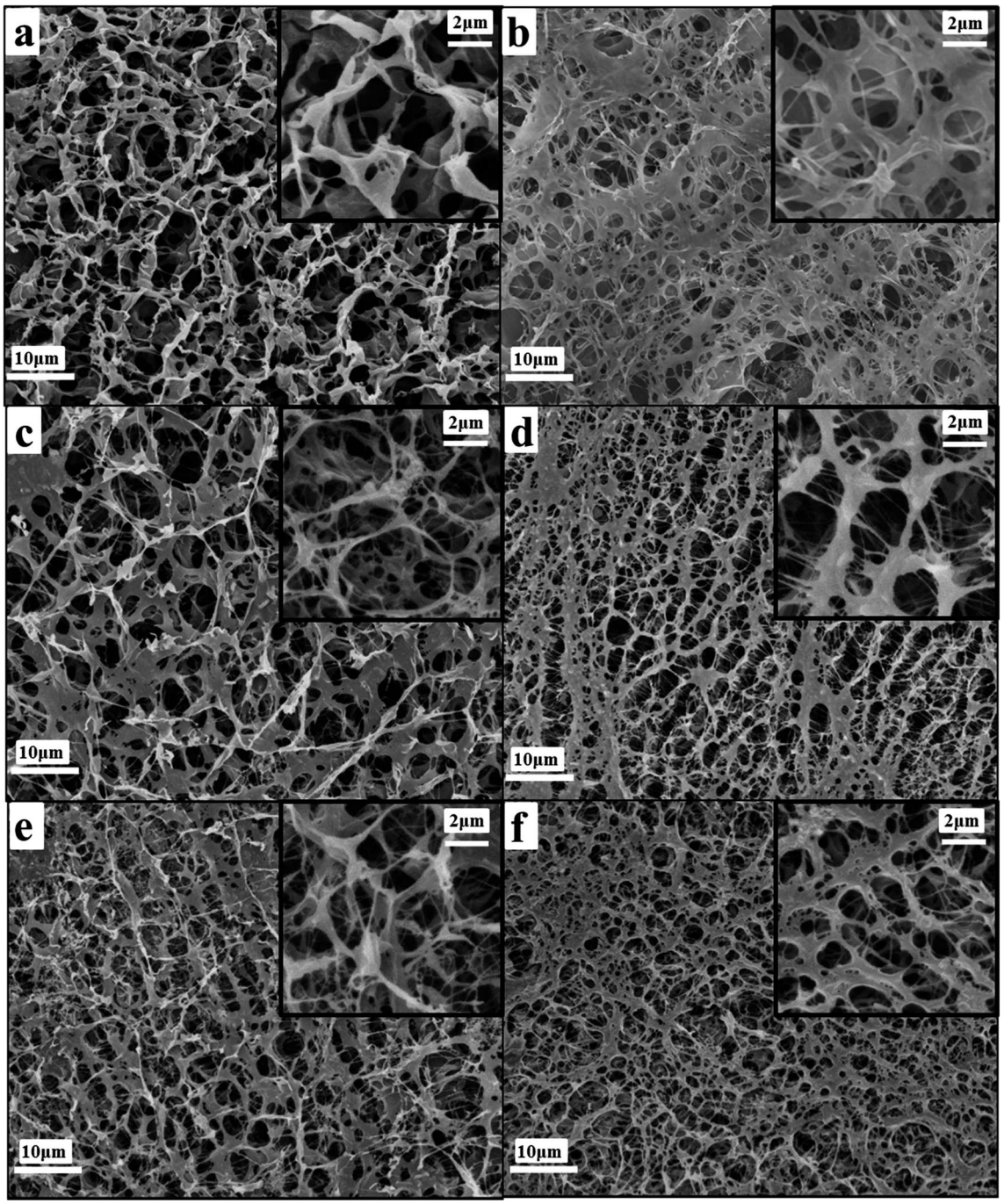

Fig. 3 SEM images of (a) PVA (25.42 kg m^{-3}), (b) PVA–CNF (26.83 kg m^{-3}), and PVA–CNF–MWCNT-1, 2, 3, and 4 aerogels prepared by a freeze-drying method with a density of (c) 14.55, (d) 20.13, (e) 26.00, and (f) 30.62 kg m^{-3}, respectively.

aerogels likely due to the small pore sizes as well as the high surface areas associated with CNFs and MWCNTs.[14,44] The surface areas of the PVA–CNF–MWCNT aerogels decreased slightly with an increasing aerogel density, which may be attributed to the lower porosity at higher densities.

Mechanical properties of the aerogels

Fig. 4(a) shows the compression stress–strain curves for the PVA, PVA–CNF, and PVA–CNF–MWCNT-3 aerogels with similar densities (~26 kg m^{-3}). The compressive modulus of the PVA–CNF aerogels (16 wt% CNFs, 150 kPa) was more than eight times higher than that of the pure PVA aerogels (17 kPa). This dramatic increase may be attributed to two factors: (1) the CNFs had excellent mechanical properties making them a desirable reinforcing nanofiller for polymers,[35,45] (2) cross-linking between the uniformly dispersed CNFs and PVA through a reaction between the hydroxyl groups present on both CNFs and PVA with the glutaraldehyde crosslinker further strengthened the hybrid aerogels. The addition of a small

Table 1 Physical and mechanical properties of aerogels prepared by the freeze-drying method

Sample	Density (kg m^{-3})	Relative density (ρ^*/ρ_s)	Young's modulus (kPa)	Yield stress (kPa)	S_{BET} (m^2 g^{-1})
PVA	25.42 ± 0.85	—	17 ± 3	3.9 ± 0.3	79 ± 6
PVA–CNF	26.83 ± 1.01	—	150 ± 11	22.6 ± 1.4	156 ± 12
PVA–CNF–MWCNT-1	14.55 ± 0.78	0.01104	54 ± 5	8.8 ± 0.7	196 ± 17
PVA–CNF–MWCNT-2	20.13 ± 0.65	0.01528	142 ± 9	18.5 ± 0.8	187 ± 15
PVA–CNF–MWCNT-3	26.00 ± 0.73	0.01974	302 ± 7	32.3 ± 0.6	181 ± 16
PVA–CNF–MWCNT-4	30.62 ± 1.19	0.02325	494 ± 15	47.5 ± 1.4	175 ± 20

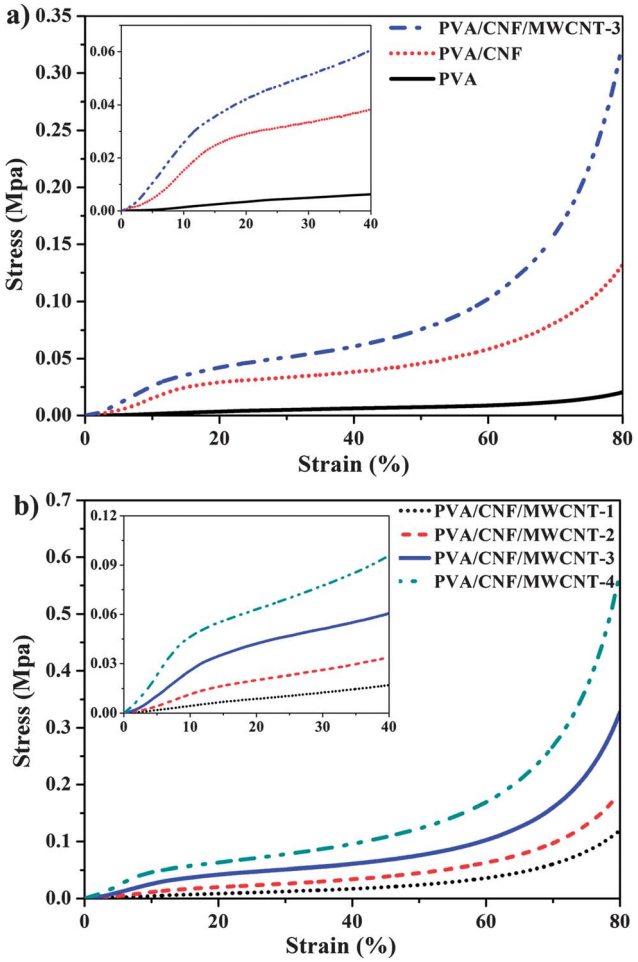

Fig. 4 (a) Compression stress–strain curves of PVA, PVA–CNF, and PVA–CNF–MWCNT-3 aerogels at similar densities (~26 kg m^{-3}); (b) Compression stress–strain curves of PVA–CNF–MWCNT aerogels with different densities.

amount of hydroxyl-functionalized MWCNTs (4 wt%) further increased the compressive modulus of the aerogels (*i.e.*, PVA–CNF–MWCNT-3) from 150 kPa to 302 kPa, accounting for the twofold increase. Similar to CNFs, MWCNTs also exhibit excellent mechanical properties and thus are a desirable reinforcing nanofiller.[32,33] Furthermore, CNFs and MWCNTs both have high aspect ratios, making it possible for them to form an entangled 3D network in the aerogels. Lastly, these MWCNTs were functionalized with hydroxyl groups, thereby enabling them to be covalently integrated into the PVA–CNF–MWCNT network through the crosslinking reaction. Fig. 4(b) shows the compression stress–strain curves of the PVA–CNF–MWCNT aerogels at different densities. Similar to other elastomeric foams,[46] three characteristic deformation regions can be observed in the these curves: (1) a linear elastic deformation region at low strain due to elastic wall bending, (2) a plateau region with slowly increasing stress after reaching a yield stress due to plastic yielding of the cell wall material, and (3) a densification region at higher strain where the stress rose sharply with the strain due to densification of the porous structures.

The mechanical properties of the PVA–CNF–MWCNT aerogels are summarized in Table 1. They had a strong dependence on density. For instance, the Young's modulus and yield stress of PVA–CNF–MWCNT-4 (30.62 kg m^{-3}) was more than 9- and 5-fold higher, respectively, than those of the PVA–CNF–MWCNT-1 (14.55 kg m^{-3}). The modulus of the PVA–CNF–MWCNT-4 aerogels (30.62 kg m^{-3}) was 494 kPa, which was more than 6-fold higher than that of the polymer/clay/nanotube aerogels with a density of 30 kg m^{-3} (79 kPa).[41] To establish the correlation between the mechanical properties (*i.e.*, the Young's modulus (E^*) and yield stress (σ^*)) of the PVA–CNF–MWCNT aerogels with their relative densities (ρ^*/ρ_s), Fig. 5 was plotted. The densities of the solid materials (ρ_s) were calculated according to the solid density of each component and their weight ratios used in the formulation. The Young's modulus E^* and yield stress σ^* were found to scale with the relative density exponentially, namely, $E^* \sim (\rho^*/\rho_s)^{2.95}$ and $\sigma^* \sim (\rho^*/\rho_s)^{2.25}$. Similar Young's modulus and relative density correlations were reported in other types of low-density nanoporous materials with the exponent ranging from 1.8 to 3.7 depending on the microstructure and formulations of the materials.[46–51]

Thermal conductivity and thermal stability of the aerogels

The thermal conductivities for the PVA, PVA–CNF, PVA–CNF–MWCNT-2, 3, and 4 aerogels measured at room temperature were 45.32 ± 0.45, 39.58 ± 0.10, 28.58 ± 0.02, 29.26 ± 0.03, and 30.79 ± 0.03 mW m^{-1} K^{-1}, respectively, thereby making them suitable as mechanically strong, ultralight thermal insulating materials. The high porosity and small-sized pores possessed by the aerogels resulted in a drastically lower thermal conductivity in comparison with their solid counterparts. Thermal transport in aerogels can occur *via* three mechanisms including gaseous conduction, solid conduction, and infrared radiative transfer.[2,52,53] However, it is mainly governed by the gaseous phase (air), whose thermal transportation rate is significantly lower

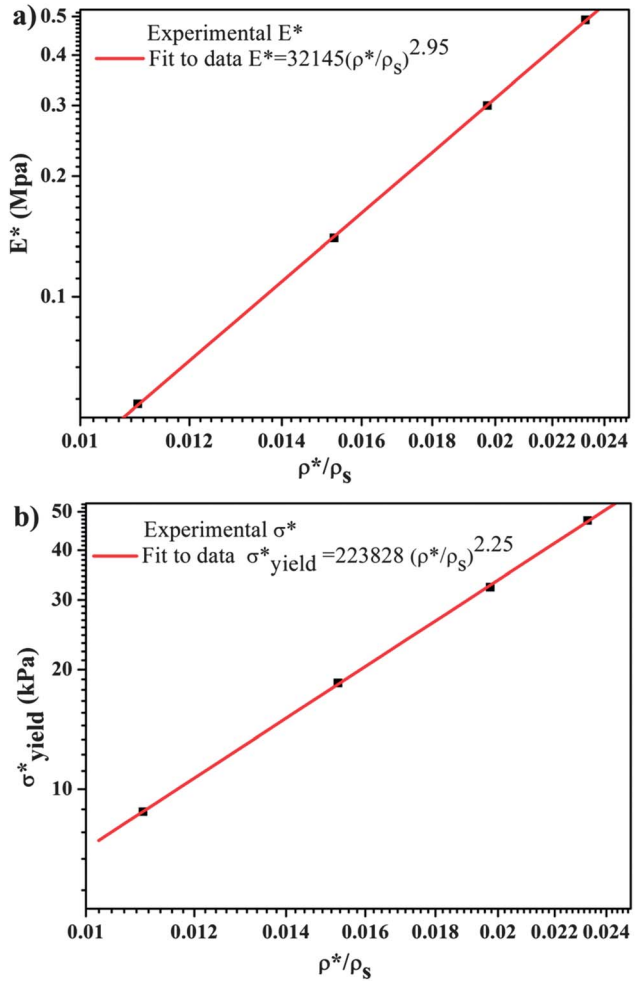

Fig. 5 Exponential correlation between (a) the Young's modulus (E^*) or (b) the yield stress (σ^*) and relatively density (ρ^*/ρ_s) of PVA–CNF–MWCNT aerogels.

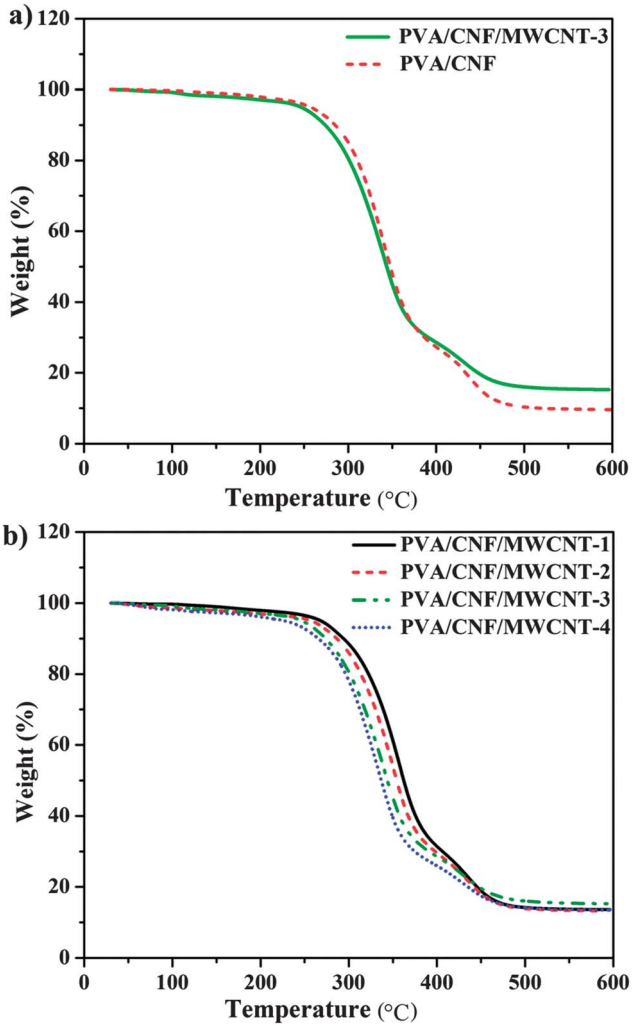

Fig. 6 (a) TGA curves of the PVA–CNF and PVA–CNF–MWCNT-3 at a similar density (~26 kg m^{-3}), and (b) TGA curves of the PVA–CNF–MWCNT aerogels at different densities.

than that by the solid phase and/or radiation. The thermal conductivities of the PVA and PVA–CNF aerogels were somewhat higher than those of the PVA–CNF–MWCNT aerogels, whose thermal conductivities did not change significantly with varying densities.

The thermal stability of the various aerogels was measured by TGA in nitrogen from 30 °C to 600 °C and is shown in Fig. 6. The thermal stability of the PVA–CNF–MWCNT aerogel decreased in comparison with the PVA–CNF aerogel as shown in Fig. 6(a). For example, the temperatures corresponding to a 10% weight loss in the PVA–CNF aerogels (287 °C) were higher than that of the PVA–CNF–MWCNT-3 (274 °C). This may be attributed to the PVA–CNF–MWCNT aerogel's higher BET surface area as compared to PVA–CNF, making it more susceptible to thermal degradation.[54] The PVA–CNF–MWCNT aerogels produced 4 wt% more carbonaceous residues after thermal degradation, which was equivalent to the amount of MWCNTs incorporated in the PVA–CNF–MWCNT aerogels. The thermal stability of the PVA–CNF–MWCNT aerogels decreased slightly with increasing density (Fig. 6(b)), which may be attributed to higher thermal conductivities at higher aerogel densities.

Conclusion

High-performance "green" PVA–CNF–MWCNT hybrid organic aerogels were prepared using an inexpensive and environmentally friendly method with renewable materials. These unique PVA–CNF–MWCNT hybrid aerogels had ultra-low densities (<31 kg m^{-3}), high surface areas (160–200 m^2 g^{-1}), and very low thermal conductivities (<31 mW m^{-1} K^{-1}). Moreover, the PVA–CNF–MWCNT hybrid organic aerogels demonstrated excellent mechanical properties, which can be attributed to the excellent mechanical properties of CNFs and MWCNTs, and the strong interactions between PVA, CNF, and MWCNTs *via* both chemical crosslinking and the formation of entangled 3D networks. The mechanical properties of the PVA–CNF–MWCNT aerogels had an exponential correlation with their relative densities. These environmentally friendly and mechanically robust aerogels can potentially be used for a wide range of applications including thermal insulation, structural components, and catalyst supports. We are currently in the process of developing

various surface functionalization techniques which will allow us to easily control the hydrophobicity of the aerogels' surfaces.

Acknowledgements

The authors gratefully acknowledge financial support from the National Science Foundation (CMMI 1032186) and the USDA Forest Products Laboratory (Madison, WI). The authors are also thankful to Professor Eric R. Roden for providing access to the BET surface area analyzer.

References

1 C. Tan, B. M. Fung, J. K. Newman and C. Vu, *Adv. Mater.*, 2001, **13**, 644–646.
2 N. Hüsing and U. Schubert, *Angew. Chem., Int. Ed.*, 1998, **37**, 22–45.
3 H. D. Gesser and P. C. Goswami, *Chem. Rev.*, 1989, **89**, 765–788.
4 L. W. Hrubesh and R. W. Pekala, *J. Mater. Res.*, 1994, **9**, 731–738.
5 J. Gross, J. Fricke and L. W. Hrubesh, *J. Acoust. Soc. Am.*, 1992, **91**, 2004–2006.
6 A. C. Pierre and G. M. Pajonk, *Chem. Rev.*, 2002, **102**, 4243–4265.
7 C. M. Castilla and F. J. M. Hodar, *Carbon*, 2005, **43**, 455–465.
8 T. Mehling, I. Smirnova, U. Guenther and R. H. H. Neubert, *J. Non-Cryst. Solids*, 2009, **355**, 2472–2479.
9 C. A. Garcia-Gonzale, M. Alnaief and I. Smirnova, *Carbohydr. Polym.*, 2011, **86**, 1425–1438.
10 J. P. Randall, M. A. B. Meador and S. C. Jana, *ACS Appl. Mater. Interfaces*, 2011, **3**, 613–626.
11 J. Biener, M. Stadermann, M. Suss, M. A. Worsley, M. M. Biener, K. A. Rose and T. F. Baumann, *Energy Environ. Sci.*, 2011, **4**, 656–667.
12 E. Frackowiak and F. Beguin, *Carbon*, 2001, **39**, 937–950.
13 D. Klemm, B. Heublein, H. Frink and A. Bohn, *Angew. Chem., Int. Ed.*, 2005, **44**, 3358–3393.
14 D. Klemm, F. Kramer, S. Moritz, T. Lindström, M. Ankerfors, D. Gray and A. Dorris, *Angew. Chem., Int. Ed.*, 2011, **50**, 5438–5466.
15 R. J. Moon, A. Martini, J. Nairn, J. Simonsen and J. Youngblood, *Chem. Soc. Rev.*, 2011, **40**, 3941–3994.
16 D. O. Carlsson, G. Nyström, Q. Zhou, L. A. Berglund, L. Nyholm and M. Strømme, *J. Mater. Chem.*, 2012, **22**, 19014–19024.
17 S. Iwamoto, K. Abe and H. Yano, *Biomacromolecules*, 2008, **9**, 1022–1026.
18 T. Saito, S. Kimura, Y. Nishiyama and A. Isogai, *Biomacromolecules*, 2007, **8**, 2485–2491.
19 T. Saito, M. Hirota, N. Tamura, S. Kimura, H. Fukuzumi, L. Heux and A. Isogai, *Biomacromolecules*, 2009, **10**, 1992–1996.
20 M. Paakko, M. Ankerfors, H. Kosonen, A. Nykanen, S. Ahola, M. Osterberg, J. Ruokolainen, J. Laine, P. T. Larsson, O. Ikkala and T. Lindstrom, *Biomacromolecules*, 2007, **8**, 1934–1941.
21 M. Henriksson, G. Henriksson, L. A. Berglund and T. Lindstrom, *Eur. Polym. J.*, 2007, **43**, 3434–3441.
22 P. C. S. F. Tischer, M. R. Sierakowski, H. Westfahl and C. A. Tischer, *Biomacromolecules*, 2010, **11**, 1217–1224.
23 L. Wågberg, G. Decher, M. Norgren, T. Lindström, M. Ankerfors and K. Axnäs, *Langmuir*, 2008, **24**, 784–795.
24 C. Aulin, J. Netrval, L. Wågberg and T. Lindström, *Soft Matter*, 2010, **6**, 3298–3305.
25 H. Jin, Y. Nishiyama, M. Wada and S. Kuga, *Colloids Surf., A*, 2004, **240**, 63–67.
26 W. Chen, H. Yu, Q. Liu, Y. Liu and J. Li, *Soft Matter*, 2011, **7**, 10360–10368.
27 M. Pääkkö, J. Vapaavuori, R. Silvennoinen, H. Kosonen, M. Ankerfors, T. Lindström, L. A. Berglund and O. Ikkala, *Soft Matter*, 2008, **4**, 2492–2499.
28 F. Fischer, A. Rigacci, R. Pirard, S. Berthon-Frbry and P. Achard, *Polymer*, 2006, **47**, 7636–7645.
29 J. Cai, S. Liu, J. Feng, S. Kimura, M. Wada, S. Kuga and L. Zhang, *Angew. Chem., Int. Ed.*, 2012, **51**, 2076–2079.
30 C. A. Morris, M. L. Anderson, R. M. Stroud, C. I. Merzbacher and D. R. Rolison, *Science*, 1999, **284**, 622–624.
31 P. M. Ajayan, *Chem. Rev.*, 1999, **99**, 1787–1799.
32 J. N. Coleman, U. Khan and Y. K. Guo'Ko, *Adv. Mater.*, 2006, **18**, 689–706.
33 Y. Hou, J. Tang, H. Zhang, C. Qian, Y. Feng and J. Liu, *ACS Nano*, 2009, **3**, 1057–1062.
34 M. G. Adsul, D. A. Rey and D. V. Gokhale, *J. Mater. Chem.*, 2011, **21**, 2054–2056.
35 R. Endo, T. Saito and A. Isogai, *Polymer*, 2013, **54**, 935–941.
36 A. Javadi, Q. Zheng, F. Payen, A. Javadi, Y. Altin, Z. Cai, R. Salo and S. Gong, *ACS Appl. Mater. Interfaces*, 2013, **5**, 5969–5975.
37 H. Tamon, H. Ishizaka, T. Yamamoto and T. Suzuki, *Carbon*, 2000, **38**, 1099–1105.
38 H. Sehaqui, Q. Zhou and L. A. Berglund, *Compos. Sci. Technol.*, 2011, **7**, 1593–1599.
39 M. D. Gawryla, O. van den Berg, C. Weder and D. A. Schiraldi, *J. Mater. Chem.*, 2009, **19**, 2118–2124.
40 E. M. Arndt, M. D. Gawryla and D. A. Schiraldi, *J. Mater. Chem.*, 2007, **17**, 3525–3529.
41 M. D. Gawryla, L. Liu, J. C. Grulan and D. A. Schirldi, *Macromol. Rapid Commun.*, 2009, **30**, 1669–1673.
42 D. J. Boday, R. J. Stover, B. Muriithi, M. W. Keller, J. T. Wertz, K. A. D. Obrey and D. A. Loy, *ACS Appl. Mater. Interfaces*, 2009, **1**, 1364–1369.
43 J. Cai, S. Kimura, M. Wada, S. Kuga and L. Zhang, *ChemSusChem*, 2008, **1**, 149–154.
44 E. Raymundo-Piñero, D. Cazorla-Amorós, A. Linares-Solano, S. Delpeux, E. Frackowiak, K. Szostak and F. Béguin, *Carbon*, 2002, **40**, 1614–1617.
45 H. Koga, T. Saito, T. Kitaoka, M. Nogi, K. Suganuma and A. Isogai, *Biomacromolecules*, 2013, **14**, 1160–1165.
46 L. J. Gibson and M. F. Ashby, *Cellular Solids: Structure and Properties*, Cambridge Univ. Press, Cambridge, England, 1997.
47 S. O. Kucheyev, T. F. Baumann, C. A. Cox, Y. M. Wang, J. H. Satcher, A. V. Hamza and J. E. Brady, *Appl. Phys. Lett.*, 2006, **89**, 041911.

48 F. Terki, J. Pelous, P. Dieudonne and T. Woignier, *J. Non-Cryst. Solids*, 1998, **225**, 277–281.
49 R. W. Pekala, C. T. Alviso and J. D. Lemay, *J. Non-Cryst. Solids*, 1990, **125**, 67–75.
50 M. A. Worsley, S. O. Kucheyev, J. H. Satcher, A. V. Hamza and T. F. Baumann, *Appl. Phys. Lett.*, 2009, **94**, 073115.
51 H. Sehaqui, M. Salajkova, Q. Zhou and L. A. Berglund, *Soft Matter*, 2010, **6**, 1824–1832.
52 J. Fricke, *J. Non-Cryst. Solids*, 1990, **121**, 188–192.
53 J. Fricke and T. Tillotson, *Thin Solid Films*, 1997, **297**, 212–223.
54 W. Zhang, Y. Zhang, C. Lu and Y. Deng, *J. Mater. Chem.*, 2012, **22**, 11642–11650.